J Appl Electrochem (2008) 38:1347–1356
DOI 10.1007/s10800-008-9570-y

ORIGINAL PAPER

Investigation of dissolution inhibitors for electrochemical mechanical planarization of copper using beta-alanine as a complexing agent

B. K. Klug · C. M. Pettit · S. Pandija · S. V. Babu · D. Roy

Received: 16 October 2007 / Revised: 1 March 2008 / Accepted: 16 April 2008 / Published online: 29 April 2008

Abstract Dissolution inhibition capabilities of benzotriazole (BTAH) and ammonium dodecyl sulfate (ADS) are investigated, in combination with β-alanine, as a complexing agent for applications in electrochemical mechanical planarization (ECMP) of copper. Cu electrodissolution is induced by linear sweep voltammetry (LSV), and Fourier transform electrochemical impedance spectroscopy (FT-EIS) is combined with LSV to examine the relative roles of the electrolyte additives in governing the surface reactions of Cu under voltage activated conditions of ECMP. The experiments focus on the electrochemical rather than mechanical component of ECMP, and are designed to probe both the individual and combined effects of BTAH and ADS on Cu electro-dissolution in the absence of abrasion.

Keywords Beta-alanine · Copper · CMP · ECMP · Impedance spectroscopy · Surfactant

1 Introduction

Electrochemical mechanical planarization (ECMP) offers certain advantages over the conventional chemical mechanical planarization (CMP) method used in the fabrication of semiconductor microchips [1–6]. Achieving an adequate combination of complexing agents and dissolution inhibitors is critical to designing efficient ECMP solutions. In ECMP of Cu, the surface layer removal step is primarily controlled by voltage activated electrodissolution, and often complexing agents are used in combination with oxidizers to promote multiple branches of these reactions [1–5]. Generally, a dissolution inhibitor is necessary in ECMP to form thin passivating films on the surface [6]. These films protect recessed regions from dissolution as the protrusions are removed by mechanical as well as chemical and electrochemical processes [1, 2]. However, all such inhibitors may not necessarily function efficiently with all the commonly used complexing agents. In addition, when used in large concentrations ($\geq$10 mM), certain dissolution inhibitors, including the commonly used benzotriazole (BTAH), tend to leave insoluble debris resulting in scratches on the finished surface [7, 8]. Due to these reasons, there has been considerable interest in recent years in developing novel combinations of complexing agents and dissolution inhibitors for CMP applications [9–11], and these efforts are now expanding to the field of ECMP [6, 7]. Our present report addresses this subject of dissolution inhibition for ECMP of Cu using low concentrations of BTAH (1–5 mM) and an anionic surfactant, ammonium dodecyl sulfate (ADS), in combination with a relatively less explored complexing agent, β-alanine (3-aminopropionic acid).

Previously we have studied the general surface chemistries of BTAH and ADS for CMP and ECMP of Cu using glycine as a complexing agent [6–8]. More recently, we have tested β-alanine as an alternative complexing agent of glycine [12], together with ADS and BTAH used as inhibitors for CMP of Cu [13]. In our present work, we extend our

B. K. Klug · D. Roy (✉)
Department of Physics, Clarkson University, Potsdam, NY 13699-5820, USA
e-mail: samoy@clarkson.edu

C. M. Pettit
Department of Physics, Emporia State University, P.O. Box 4030, Emporia, KS 66801-5087, USA

S. Pandija · S. V. Babu
Center for Advanced Materials Processing, Clarkson University, Potsdam, NY 13699-5665, USA

investigation of the β-alanine system to the case of *voltage activated* Cu dissolution for ECMP. The advantage of using β-alanine as a complexing agent is that it might be useful to increase the polish rates while maintaining relatively low Cu dissolution, which is a main requirement for achieving high planarization efficiencies. This has been noted in a recent study, where β-alanine in comparison with glycine (at pH = 4.0) was found to yield lower dissolution rates but similar polish rates in CMP of Cu [12, 13]. This effect has been attributed to the increased chain length of β-alanine, based on the observation that the degree of complex formation by Cu and Cu oxides with certain amino acids decreased with increasing distances between the functional groups of the amino acid molecules [12, 14].

Electrodissolution of Cu (a coupon electrode) is induced in this work by applying linear sweep voltammetry (LSV). ADS is used at 3 mM concentration, where dense surface aggregates of dodecyl sulfate (DS^-) hemi-micelles are formed [7]. The surface protection efficiency of ADS on Cu is compared with those of BTAH and a mixed inhibitor system, 1 mM BTAH + 3 mM ADS. Thus, five different sets of measurements are performed (all at pH = 4.0) using: (a) A reference solution (Ref) of 0.13 M β-alanine + 0.8 wt% H_2O_2 (oxidizer); (b) Ref + 1 mM BTAH; (c) Ref + 5 mM BTAH; (d) Ref + 3 mM ADS; (e) Ref + 1 mM BTAH + 3 mM ADS. The experiments involve LSV, linear polarization resistance (LPR) measurement, and Fourier-transform electrochemical impedance spectroscopy (FT-EIS). The main utility of FT-EIS in this study is that it allows rapid collection (typically in 1 s) of full impedance spectra in the presence of interfacial reactions, avoiding any measurable surface modifications during data recording [15]. Electrode equivalent circuits (EECs) representing different branches of simultaneously occurring surface reactions are obtained from complex nonlinear least square (CNLS) analysis of the EIS data [16]. A reaction scheme is proposed to explain the relative roles of the complexing agent, the corrosion inhibitors, and the oxidizer (H_2O_2) in controlling dissolution and passivation of the Cu surface.

2 Experimental

2.1 Materials

Cu coupons (99.999% pure, from Alfa Aesar) of rectangular shapes (1.7 × 1.6 cm^2 area, 0.1 cm thickness) were used as working electrodes (WE) in a three-electrode glass cell with a Pt counter electrode and a reference saturated calomel electrode (SCE). A modified alligator clip provided electrical connection to the WE through the upper part (not dipped in the electrolyte) of the Cu coupon. Electrolytes were prepared using saturated water triply distilled in our laboratory and reagent grade (as received) chemicals from Aldrich. Due to the generation of Cu^{2+} ions during dissolution experiments, the solutions were replaced by fresh electrolytes before each electrochemical measurement. Between subsequent tests, the Cu sample was polished on a home-built polisher using a paste of 1 μm alumina abrasives and triply distilled water on a rotating stainless steel base covered with Buehler Microcloth™, followed by thorough rinsing with triply distilled water.

2.2 Instrumentation and procedures

EIS was performed between 40 KHz and 100 Hz, with the lower limit set according to the criteria for time resolved FT-EIS [15]. The amplitudes (2.5 mV) and frequencies of the 190 sinusoidal waves in the AC perturbation spectrum were selected at appropriate intervals according to considerations of response sensitive perturbation [15]. The AC perturbation voltage was a computer-generated noise-like signal, applied through the digital/analog conversion channels of a data acquisition card from National Instruments. Virtual instrument (VI™) codes developed by our group using LabVIEW™ were used to control the experiments and to store data. The chrip-z algorithm for Discrete Fourier Transform was used to process the impedance spectra. Real (Z') and imaginary (Z'') parts of the measured impedance were used to obtain Nyquist spectra. The Nyquist spectra were subjected to CNLS fitting to trial electrode equivalent circuit (EEC) models using ZSimpWin™, and only those circuit models resulting in ≤5% uncertainties in calculated impedance elements were accepted.

Since FT-EIS was used in this work in the time-resolved (rather than the long-integration) mode, the lower limit of the AC perturbation signal was constrained at 100 Hz. This did not allow for polarization resistance measurement through EIS (which would require low frequency AC perturbation, at least down to 1 Hz). Therefore, linear polarization resistances were measured using DC LSV. The mass of the Cu sample was measured at different steps of the experiments, and the solution pH also was monitored both before and after each LSV treatment (with accuracies of 0.01 unit and 0.01 mg, respectively). Electrochemical dissolution rates were calculated by measuring the electrode mass before and after LSV activation, and by using the mass-difference data as discussed previously [4].

3 Results and discussion

3.1 Corrosion parameters

Figure 1 shows polarization (Tafel) plots for a Cu coupon electrode in different solutions, where the corrosion

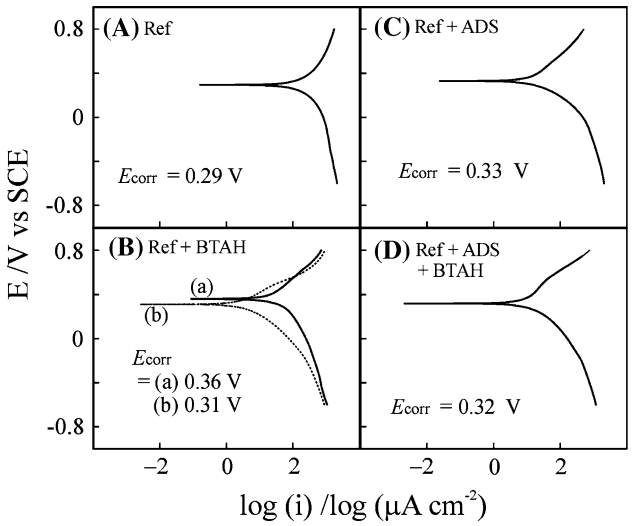

Fig. 1 Potentiodynamic polarization (Tafel) plots for a Cu coupon electrode, recorded by sweeping the voltage at 5 mV s^{-1} from −0.6 to 0.8 V in different solutions. *E* and *i* represent the voltage and the current, respectively. Ref = 0.13 M *β*-alanine + 0.8 wt% H_2O_2. ADS concentration is 3 mM in C and D. BTAH concentrations 1 mM for plots B (a) and D, and 5 mM for B (b)

potentials (E_{corr}) are indicated. E_{corr} values, in combination with those of the corrosion currents (i_{corr}) often are taken as qualitative measures of surface reactivity. However, for multi-component CMP and ECMP solutions supporting several mutually parallel faradaic reactions, this approach may not always indicate the reactive/passive nature of the electrode surface in a straightforward way. For instance, surface oxides on Cu generally shift E_{corr} in the anodic direction, and at the same time, these oxides tend to dissolve by reacting with the complexing agent(s) present in the solution [9]. The E_{corr} values in such cases are affected in a rather nontrivial manner by both the surface-oxide and complex films. This effect can be rather problematic in the measurement of Tafel plots where relatively large overpotentials are applied allowing for the activation of different charge transfer reactions over a sizable voltage range [17]. The situation is further complicated if the surface passivating agent (like BTAH) not only shifts E_{corr} but also contributes to the measured faradaic currents when potentiodynamic polarization is applied. Under these conditions, the trends observed in the values of i_{corr} are unlikely to show any obvious correlations with those of E_{corr}.

Because the presently used systems include faradaically reactive BTAH on Cu, in view of the above considerations, we use an additional DC method, namely that of linear polarization resistance (LPR) measurement to evaluate the surface reactivity and passivity of Cu. LPR monitoring usually is performed close to E_{corr} where the current-overvoltage plots are linear, and R_p is determined using the Stern–Geary approach [17]: $R_p = \mathrm{Lim}_{\eta\to 0}\,(\mathrm{d}i/\mathrm{d}\eta)^{-1}$, with η representing the overpotential, $(E-E_{corr})$. The LPR measurements performed in the present study also are based on this principle, but at the same time are designed to incorporate the effects of surface modifications that would occur in the full range of voltage activation for ECMP. This is achieved by scanning the applied voltage 0.0 → −0.6 → 0.8 V (range used here to activate electro-dissolution) at 5 mVs^{-1}, and by using the linear regions ($E_{corr} \pm 0.05$ V) of the resulting voltammograms for LPR measurements. These linear (i–η) data (symbols) are shown in Fig. 2, and the lines represent fits to the data to obtain the slopes ($\mathrm{d}i/\mathrm{d}\eta$). It is useful to note here how the current scale drops drastically in going from the inhibitor free (A) to the inhibitor containing (B–D) systems.

In Fig. 3A and B, we compare the solution dependent values of i_{corr} and R_p, respectively. A comparison of i_{corr} with E_{corr} in Fig. 1 indicates a lack of correlation between the trends of the two sets of results. As explained above, this is not surprising considering the faradaic nature of Cu-BTA complex formation reaction [7]. In Fig. 3, however, a strong correlation is found between the solution dependent values of i_{corr} and R_p. For the four inhibitor containing solutions, b (Ref + 1 mM BTAH), c (Ref + 5 mM BTAH), d (Ref + 3 mM ADS) and e (Ref + 1 mM BTAH + 3 mM ADS), the i_{corr} values appear in the order i_{corr} (c) < i_{corr} (e) < i_{corr} (d) < i_{corr} (b), and the polarization conductance ($1/R_p$) from Fig. 3B follows this same order. Based on this observation, we take i_{corr} and ($1/R_p$) as the main parameters indicating *electrochemically measured* inhibition efficiencies (*IE*) of the dissolution inhibitors used here.

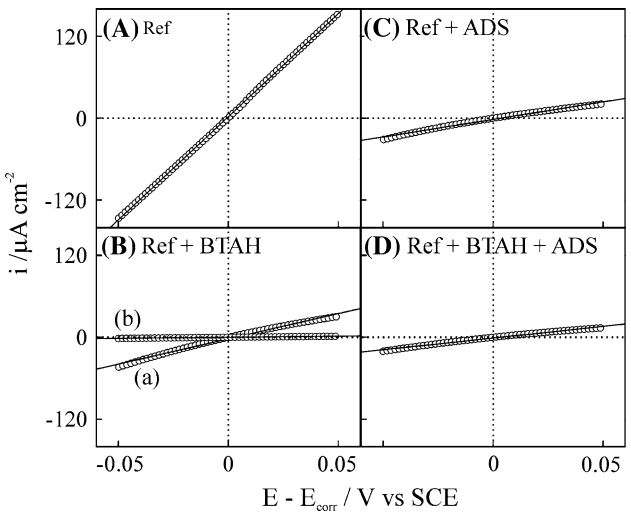

Fig. 2 Current (*i*) versus overpotential (E–E_{corr}) plots used to determine the DC linear polarization resistance of a Cu electrode. The different electrolytes in (A–D) are the same as those indicated in the corresponding panels of Fig. 1. The symbols are experimental data and the lines are linear fits to the data

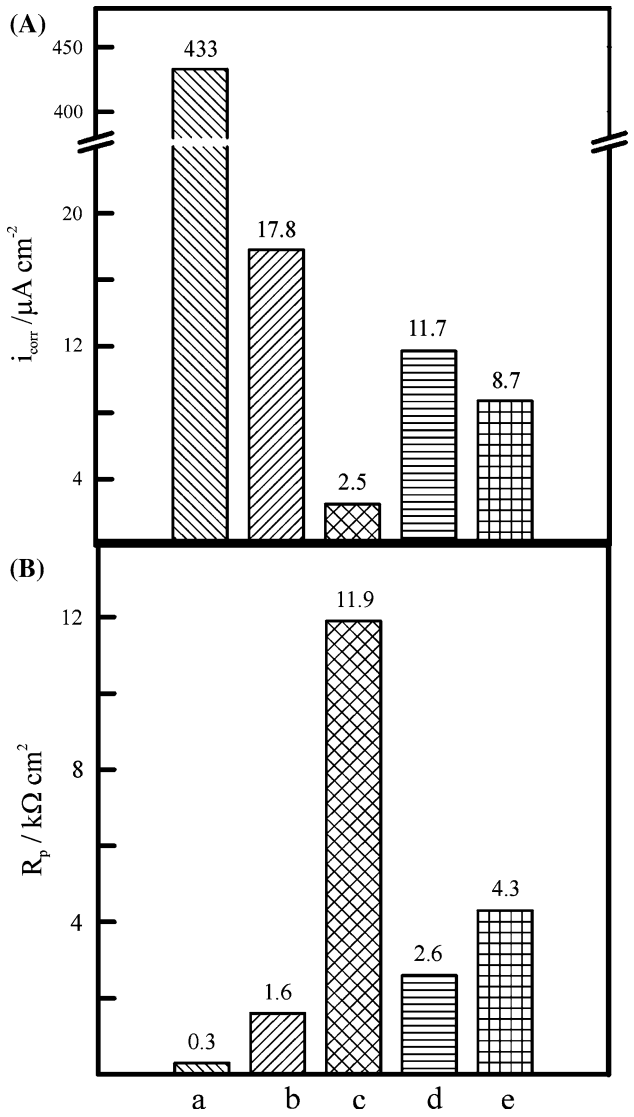

Fig. 3 (A) Corrosion currents i_{corr} and (B) DC polarization resistances R_p of a Cu electrode in (a) 0.13 M β-alanine + 0.8 wt% H_2O_2. (Ref), (b) Ref + 1 mM BTAH, (c) Ref + 5 mM BTAH, (d) Ref + 3 mM ADS and (e) Ref + 1 mM BTAH + 3 mM ADS. The values of the measured quantities are indicated at the top of the corresponding bars

3.2 Surface reactions in the absence of dissolution inhibitors

Let us examine the surface reactions of Cu that give rise to the polarization currents observed in Fig. 1A in the absence of the dissolution inhibitors. Anodic dissolution of Cu in the form of Cu^{2+} occurs as follows [4]:

$$Cu = Cu^{2+} + 2e^{-}. \quad (1)$$

The H_2O_2 in the solution acts to anodically dissolve Cu,

$$Cu + H_2O_2 + 2H^{+} = Cu^{2+} + 2H_2O, \quad (2)$$

and at the same time, oxidizes bare surface areas of Cu. At the 0.8 wt% H_2O_2 content of the experimental solution, the predominant oxide species is Cu_2O [18, 19]: $2Cu + H_2O_2 = Cu_2O + H_2O$. This Cu_2O can be dissolved by the complexing agent β-alanine as noted below. At pH = 4.0, β-alanine exists predominantly in the form of HL (L ≡ $H_2NCH_2CH_2COO$), mixed with a lesser amount of H_2L^{+} [14]. By noting that $CuHL^{2+}$ is the predominant form of the dissociated copper-β-alanine complex at pH = 4.0, we expect the following reactions in the Ref solution [12, 14]:

$$Cu_2O + 2HL + 2H^{+} = 2CuHL^{2+} + H_2O + 2e^{-}, \quad (3)$$

$$Cu + H_2L^{+} = CuHL^{2+} + 2e^{-} + H^{+}, \quad (4)$$

$$Cu + HL = CuHL^{2+} + 2e^{-}. \quad (5)$$

The anodic current branch of Fig. 1A is expected to have contributions from the charge transfer reactions (1) and (3–5). The corresponding cathodic branch should have a significant contribution of oxygen reduction [3, 4]:

$$O_2 + 4H^{+} + 4e^{-} = 2H_2O. \quad (6)$$

The relative roles of the complexing agent and the oxidizer in governing electrodissolution of Cu can be noted from the above reactions. Without H_2O_2 and β-alanine, the only likely channel (at pH = 4.0) for copper electrodissolution would be in the form of Cu^{2+} via Eq. 1. The additional routes of Cu^{2+} dissolution in Eq. 2 become available in the presence of H_2O_2. β-alanine introduces further surface dissolution in the form of $CuHL^{2+}$ through reactions (4) and (5). The combined effects of H_2O_2 and β-alanine are manifested in reaction (3), where the Cu_2O, eventually dissolved by β-alanine, is initially formed by H_2O_2.

3.3 Surface reactions in the presence of dissolution inhibitors

At pH = 4.0, BTAH exists in its neutral form, and can nonfaradaically adsorb on both Cu and Cu_2O [20, 21]. The thickness of this chemisorbed film, denoted here as $(BTAH)^{ad}$, generally is restricted to a monolayer and at low solution concentrations (~1 mM) of BTAH [7]. Anodic formation of the Cu–BTA complex occurs at relatively higher BTAH concentrations (often at >5 mM) [21–23]: Cu + BTAH = Cu-BTA + H^{+} + e^{-}. The Cu–BTA complex can grow beyond a monolayer, and depending on the magnitude and duration of the applied voltage, can polymerize to build strong surface passivating films [21–23]. In addition, the anodic current contribution of Cu–BTA formation can affect the analysis of corrosion parameters in BTAH containing systems.

In ADS containing solutions, the dissolved DS^{-} anions adsorb nonfaradaically on Cu as well as on Cu-oxides [7]. This absorption mechanism is governed by electrostatic interactions between the positively charged Cu/Cu-oxide surface (at pH = 4.0) and the DS^{-} anions [6–8]. At the

3 mM concentration of ADS used here, the adsorbed species take the form of densely packed hemimicelles, $(DS^-)^{ad}_n$, where n is the number of DS^- ions in each unit cell [6, 8].

The surface films of $(BTAH)^{ad}$, Cu–BTA and $(DS^-)^{ad}_n$ can block Cu dissolution under the OCP conditions of CMP, and this subject has been discussed in detail in our earlier papers [6–8]. At a sufficient cathodic overpotential, the electron transfer step of Eq. 6 could occur at a measurable rate through minor pinholes in the oxide and/or dissolution inhibitor films. On the other hand, for the reactions (2–5) to occur, the Cu surface must be in direct contact with the solution species, and the availability of this condition becomes limited even at moderate anodic overpotentials as the inhibitor surface films are formed. Similarly, reaction (1) requires an intermediate step of activated complex formation involving direct adsorption of H_2O molecules on Cu [24]; this process would also be hindered in the presence of hydrophobic BTAH and/or $(DS^-)^{ad}_n$ films. Dissolution of Cu_2O (Eq. 3) would be similarly restricted by the $(BTAH)^{ad}$ and/or $(DS^-)^{ad}_n$ films formed on Cu_2O. In view of these considerations, anodic dissolution of Cu should be largely limited by the inhibitor films, whereas the faradaic processes activated at cathodic overpotentials might still remain operative to a certain extent. In fact, a careful examination of Fig. 1 indicates that the overall shapes of the cathodic branches in Fig. 1 are similar among the five different solutions used, suggesting that the cathodic Tafel branches are dominated by a common reaction as suggested in Eq. 6.

3.4 Voltage activated removal of Cu surface layers using linear sweep voltammetry

Different voltage- and current-controlled activation schemes, including pulse modulation, DC step and LSV methods can be used for electro-dissolution of Cu in ECMP [1–6, 25]. In the present work, we use the LSV scheme (ranging between −0.6 and 0.8 V, scanned at 5 mV s^{-1}), described in the caption of Fig. 4. This voltage activates anodic dissolution reactions above E_{corr} during the positive scan; the reversed scans extending into the cathodic region are included to avoid rapid buildup of dissolved electro-dissolved Cu^{2+} in front of the electrode surface (which often occurs under continuous application of strong anodic potentials [4], and subsequently tends to shift E_{corr} *during* the experiment). The solution dependent electrode currents are shown in Fig. 4A–D.

The anodic currents in Fig. 4 are more effectively suppressed than the cathodic currents. This reinforces the point we mentioned at the end of Sect. 3.3, that the cathodic currents observed here are largely supported by reaction (6), and that contributions of the reverse steps of the anodic dissolution reactions to this current are comparatively

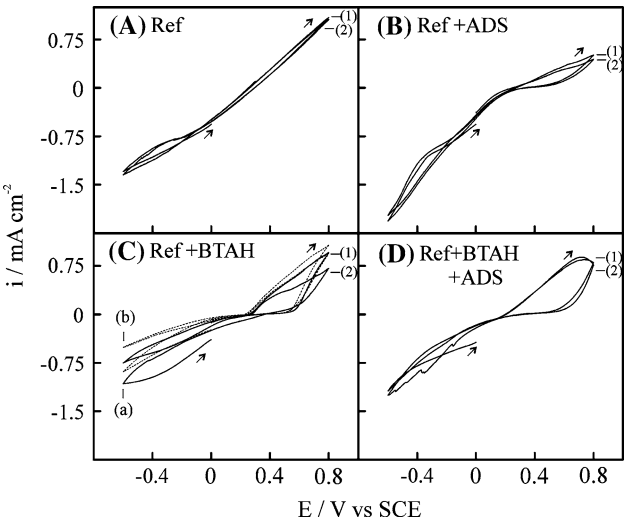

Fig. 4 Voltage dependent electro-dissolution currents of Cu, recorded in different solutions by applying two successive cycles of a linear sweep voltage program, 0 → −0.6 → 0.8 V at 5 mV s^{-1}. Cycles (1) and (2) are identified on the plots, and the arrows indicate the direction of voltage scan. Ref = 0.13 M β-alanine + 0.8 wt% H_2O_2. In (C), plots (a) and (b) correspond to BTAH concentrations of 5 and 1 mM, respectively

small. This in turn, implies that in spite of the cathodic voltage region allowed in the activation profile, the anodic dissolution reactions have sizable components that are irreversible with respect to voltage reversal. In other words, during a given LSV cycle, the net amount of Cu^{2+} and $CuHL^{2+}$ dissolved should be larger than the corresponding (if any) re-deposited amounts of these species on to the surface. Thus, a net loss in the sample mass is expected following the LSV treatment, and this is what we observe in the removal rate (RR) data shown in Fig. 5.

The open bars in Fig. 5 are nominal RR values, based on the quantity $(\Delta m/T)$, where Δm is the loss in sample mass due to a full activation treatment (0.0 → −0.6 → 0.8 → −0.6 → 0.8 → −0.6 → 0.0 V), and T is the total time of this treatment. The shaded bars in Fig. 5 represent scaled RR values, normalized as $(\Delta m/T_a)$, where T_a is the net time that the sample actually spends above E_{corr} during the applied LSV profile. This normalized RR is a more representative parameter of ECMP efficiency than the nominal RR, because anodic dissolution reactions stop when the voltage of the LSV drop below E_{corr}.

Based on the results of the electrochemical measurements, we define the percentile dissolution inhibition efficiency (IE) of a given inhibitor as

$$IE = \frac{[1/R_p(0)] - [1/R_p]}{[1/R_p(0)]} \times 100, \quad (7)$$

where $[1/R_p(0)]$ and $[1/R_p]$ are the polarization conductances measured in the absence and in the presence of the inhibitor additive, respectively; $R_p(0)$ and R_p are the

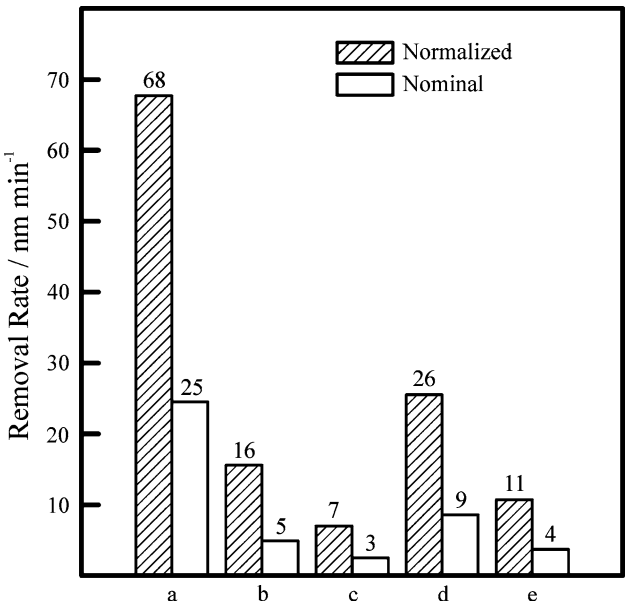

Fig. 5 Rates of electrochemical removal of Cu surface layers, induced by LSV. The electrolytes labelled (a–e) are the same as those labeled correspondingly in Fig. 3. The nominal removal rates are calculated by dividing the electrochemically induced mass loss of the sample by the total time of the applied voltage sweep. Normalized removal rates are calculated by replacing this interval with the actual anodic activation time during which the sweep voltage remains above E_{corr}

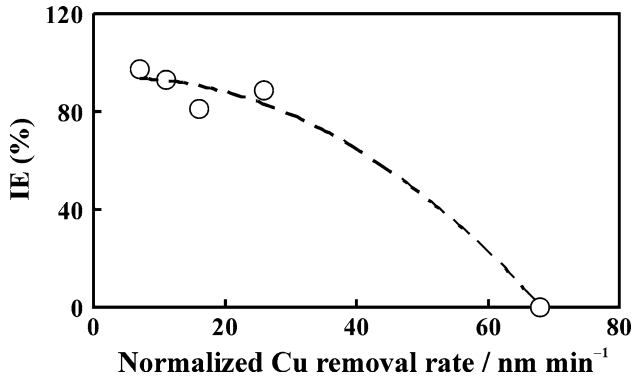

Fig. 6 Normalized Cu removal rates (taken from Fig. 5), correlated with the inhibition efficiency parameter IE (calculated from Eq. 7 using the R_p data of Fig. 3)

corresponding polarization resistances. In Fig. 6, we plot *IE* values, evaluated using Eq. 7 and the R_p data from Fig. 3, against the normalized Cu removal rates from Fig. 5. The symbols in Fig. 6 are data points and the line through the symbols is included to show the general trend of the data. As expected, a clear correlation is observed between the electrochemical and the mass-loss data in Fig. 6.

To ensure that the electrolyte composition did not change due to any cumulative irreversible surface reactions during LSV, we monitored the solution pH before (pH_i) and after (pH_f) each LSV treatment of the sample. The measured pH differences, $\Delta pH = (pH_f\text{-}pH_i)$, for the different solutions are listed in Table 1, and these changes can be considered negligible. This observation is consistent with the reaction scheme described above, according to which, H^+ ions are generated by reaction (4) and are consumed by reactions (2, 3) and (6).

In addition to promoting strong surface passivation, an effective dissolution inhibitor for ECMP (and CMP) should provide predominantly defect-free processed surfaces. We have discussed this topic elsewhere in detail for the presently used β-alanine/ADS/BTAH system [13]. Based on our earlier findings, here we briefly note that Cu CMP solutions of β-alanine containing $\geq$5 mM BTAH (at pH = 4.0) tend to leave scratches on processed (at 2 psi polishing pressure) Cu wafer surfaces [13]. In comparison, 3 mM ADS used alone or mixed with $\leq$1 mM BTAH in β-alanine solutions under the same polishing conditions was found to provide good quality post-polish surfaces, while requiring a slight compromise of the overall dissolution inhibition efficiencies. Achieving this adequate balance between surface defect reduction and dissolution suppression often is more important than enhancing the latter condition alone [7, 8]. The results of Figs. 3 and 5 presented here show that in going from the 5 mM BTAH to the mixed inhibitor system 3 mM ADS + 1 mM BTAH, the absolute degree of dissolution inhibition is compromised by a relatively small amount, but reduction in surface roughness should be a significant gain in the latter case as we have shown previously [13].

3.5 Results of FT-EIS measurements

We used FT-EIS to examine if the reaction scheme proposed in the discussion of the DC electrochemical results was consistent with the AC impedance response of the Cu electrode. Our EIS strategy here is based on the observation that reactive interfaces supporting strong faradaic processes like electrodissolution can be represented in terms of the typical generalized electrode-equivalent circuit (EEC) shown in Fig. 7A [16]. Here, R_u is the uncompensated solution resistance, C_d is an effective double layer capacitance that includes a series combination of the capacitances of surface films (of oxides and/or passivating layers), and R_p is the polarization resistance providing the ohmic path for the faradaic current flow across the interface. The branch containing the general adsorption element Z_a is expected in the presence of discontinuous oxide films and specific adsorption of dissolution inhibitor adsorbates [26, 27]. EIS analysis can provide relative values of the different reaction branches (that is relative efficiencies of the surface dissolution and protection steps), as well as the

Table 1 Impedance parameters, DC polarization conductance ($1/R_p$) and LSV induced pH changes measured for a Cu coupon electrode in different solutions

	0.13 M β- alanine + 0.8 wt% H_2O_2 at pH = 4.0 [Ref solution (a)]	Ref + 1 mM BTAH [solution (b)]	Ref + 5 mM BTAH [solution (c)]	Ref + 3 mM ADS [solution (d)]	Ref + 1 mM BTAH + 3 mM ADS [solution (e)]
$R_u/\Omega\ cm^2$	1.5	1.4	1.2	1.1	1.2
$C_d/\mu F\ cm^{-2}$	0.2	1.6	1.5	1.0	1.1
$R_a/\Omega\ cm^2$	–	225	240	182	215
$\sigma_a/k\Omega\ cm^2\ s^{-0.5}$	–	1.0	1.3	2.8	3.5
$Y'_a/mS\ cm^{-2}$	0	3.69	3.21	2.97	2.44
R_p from EIS/$\Omega\ cm^2$	220	–	–	–	–
$(1/R_p)$ from DC LPR/mS cm^{-2}	3.30	0.62	0.08	0.38	0.23
ΔpH	0.01	0.00	0.01	0.00	0.00

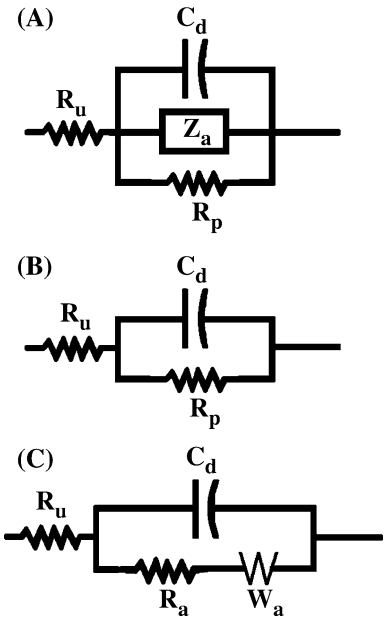

Fig. 7 Electrode equivalent circuits of Cu subjected to surface dissolution and passivation. (A) A general circuit including adsorption of solution species (middle branch) and faradaic dissolution (lowest branch). (B) Circuit used to fit experimental Nyquist plots recorded in the absence of any dissolution inhibitors in the solution. (C) Circuit used to fit experimental Nyquist plots recorded in the presence of BTAH, and/or ADS dissolution inhibitors in the solution. The elements of each circuit are described in the main text

detailed constituent elements of the adsorption branch (kinetics of the adsorption steps) [16].

FT-EIS was carried out within ± 0.05 V of E_{corr} (in the same range as that used for LPR measurements). Figure 8 shows illustrative Nyquist plots for (A) inhibitor free and (B) different inhibitor containing solutions, recorded at the respective corrosion voltages of Cu (from Fig. 1) in these solutions. Z′ and Z″ are the real and imaginary impedances. On each Nyquist plot, the right-most and left-most data points represent the lowest (100 Hz) and highest (40 KHz) frequencies of the spectrum, respectively. The Nyquist plots recorded at other voltages in the range of $E_{corr} \pm 0.05$ V do not show any significant differences, and this is illustrated by the two sets of EIS data in Fig. 9 recorded for the inhibitor containing systems at (A) $E_{corr} + 0.05$ V and (B) $E_{corr} - 0.05$ V. The symbols and the lines in both Figs. 8 and 9 represent experimental data, and CNLS fits to the data, respectively.

In the high frequency (short time scale) region (lower left corner) of Figs. 8 and 9, the impedance graphs for the different corrosion inhibitors are mutually similar, but at lower frequencies (longer times corresponding to the upper right sections of the plots), visible differences appear in their shapes and values. This indicates that the inhibitor adsorption step is a relatively slow process, and this observation is consistent with the DC (zero-frequency) results of Figs. 3 and 5, where the different effects of the different inhibitors are clearly manifested. For the Ref solution (a), all the Nyquist plots recorded in the $E_{corr} \pm 0.05$ V range showed excellent CNLS fits to the EEC of Fig. 7B; the corresponding fits for the inhibitor containing solutions (b–e) yielded the EEC of Fig. 7C. In Fig. 8A (representing the EEC of Fig. 7B), the overall Z″ values are smaller than those of Fig. 8B (representing the EEC of Fig. 7C) due to the presence of the phase sensitive Warburg element W_a in the latter case. A comparison of the overall Z′ scales in Fig. 8A, B indicates that the combined impedance of the C_d and Z_a branches in the presence of inhibitors is on the same order of magnitude of R_p measured in the Ref solution alone. According to Fig. 3, R_p increases at least by an order of magnitude as the inhibitors are introduced in the solution, and such large values of R_p would not even fit on the Z′ scale used in Fig. 8. In other words, the values of R_p in the

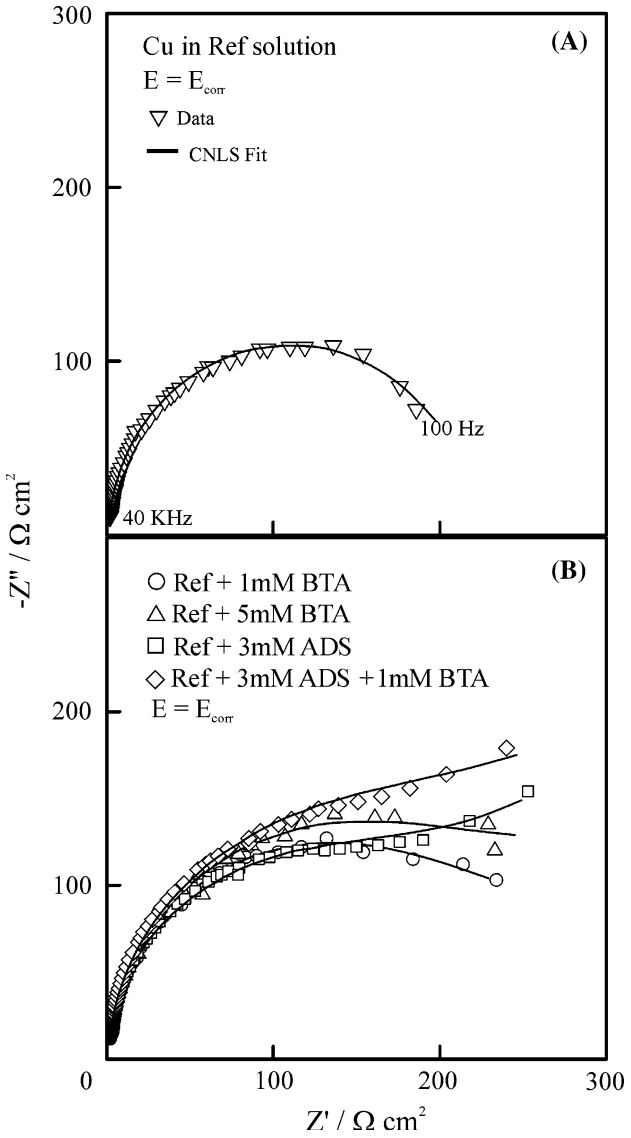

Fig. 8 Nyquist plots for Cu recorded at E_{corr} in different solutions. The detailed solution compositions are defined in Figure caption 3 as well as in the main text. The symbols represent experimental data, and the lines are CNLS fits to the data using the EEC of Fig. 7B (for the plots in A above) or 7C (for the plots in B above)

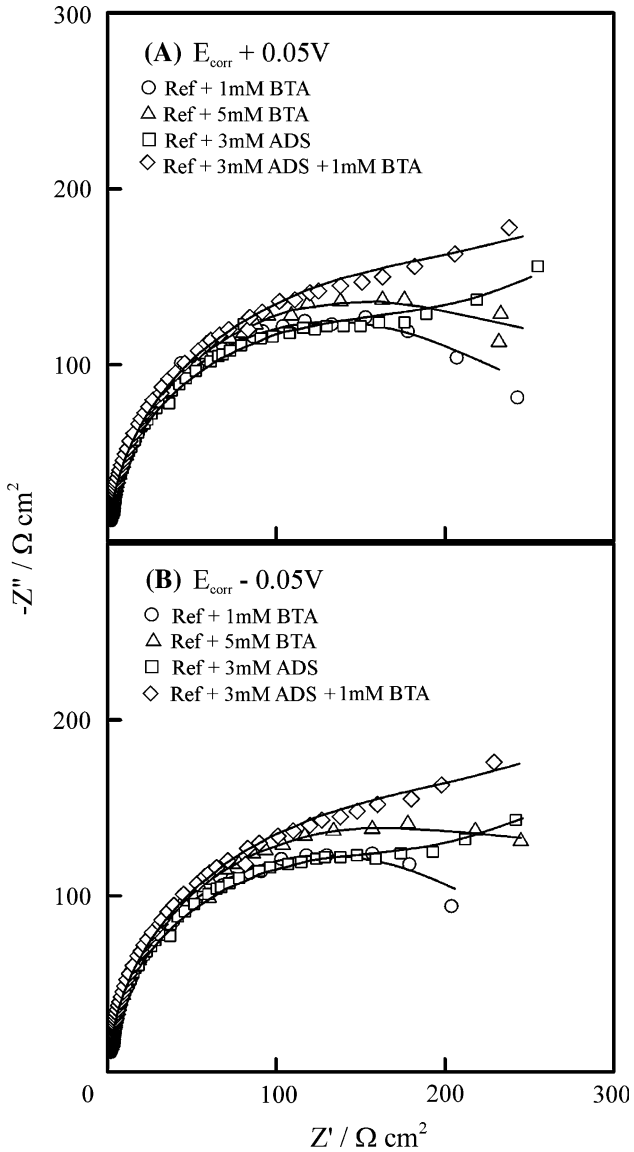

Fig. 9 Nyquist plots for Cu recorded (A) 0.05 V above and (B) 0.05 V below E_{corr} in different solutions. The detailed solution compositions are defined in Figure caption 3 as well as in the main text. The symbols represent experimental data, and the lines are CNLS fits to the data using the EEC of Fig. 7C

presence of the dissolution inhibitors are too large to be detected within the low frequency limit of FT-EIS. These observations are further clarified below in terms of the EEC models.

Figure 7B for the inhibitor free system only contains capacitive and ohmic contributions of the double layer (C_d) and faradic dissolution reactions (R_p), respectively. Z_a is infinitely large in the absence of the inhibitors. In the presence of inhibitors (Fig. 7C), the adsorption impedance Z_a is identified as a series combination of an adsorption resistance R_a (representing individual or combined chemisorption of BTAH and ADS), and a Warburg element W_a (representing semi-infinite diffusion of BTAH and/or DS^- from the bulk solution to the Cu electrode surface). The complex impedance of the Warburg element has the form [16]: $Z_{Wa} = \sigma_a(1 - j)(\omega)^{-1/2}$, where σ_a is the frequency independent component of W_a, ω is the angular frequency of the AC perturbation voltage, and $j = (-1)^{1/2}$. In Fig. 7C, R_p is not detected because as we noted above, this resistance is too large (faradaic dissolution being effectively suppressed) in the presence of the inhibitors. The R_a–W_a branch in Fig. 7C is also likely to have a series contribution from an adsorption capacitance (C_a), as often found in generalized Randles circuits [16]. However, due

to the strong adsorption characteristics of DS^- and BTAH on Cu/Cu-oxide, the effective reactance ($1/[\omega C_a]$) of such a (high) capacitance most probably is too low compared to the impedance of the R_a–W_a combination and hence, does not manifest itself in the adsorption branch in Fig. 7C.

Table 1 presents the impedance parameters obtained from CNLS analysis of the EIS data. The values of each element vary only slightly ($< \pm 3\%$) within the DC voltage range ($E_{corr} \pm 0.05$ V) explored, and the entries in Table 1 represent averaged values within this range. The values of R_u are comparable among the different solutions, implying that the solution resistance is governed mainly by the concentration of H_2L^+, which is the same for the different solutions used. The effective double layer capacitance has the form [27–29]: $C_d = [(1/C_{d0}) + (1/C_f)]^{-1}$, where C_{d0} is the diffuse layer capacitance in the absence of surface films, and C_f is the net capacitance contribution of different components of the surface films (copper oxide, complexing agent and/or inhibitor species). In Table 1, C_d is lowest for the Ref solution where the surface film is predominantly composed of copper oxides and adsorbed β-alanine. In the presence of dissolution inhibitors, C_d increases considerably. This is consistent with the above definition of C_d, and suggests that the values of C_f for the inhibitor films are higher than those for the copper oxide and complexing agent surface films. A comparison of the observed values of R_a indicates that the adsorption resistance for BTAH is somewhat higher than that of DS^- on Cu/Cu_2O.

The values of σ_a for the ADS-added solutions are noticeably higher than those of the BTAH solutions. To clarify this observation, we note that the factors governing the values of σ_a for the neutral and anionic inhibitor species in the solutions are somewhat different. At and near the OCP, the term $\sigma_a(DS^-)$ describing diffusion of the charged DS^- depends primarily on the solution concentration of the anion, whereas the corresponding term σ_a(BTAH) associated with diffusion of uncharged BTAH is affected by both the solution concentration and the rate of adsorption of the molecule [30]. Due to this reason, the σ_a terms for the two dissolution inhibitor species are unlikely to scale in the same proportionate way with respect to the values of their respective diffusion coefficients. Moreover, the considerably different molecular shapes of these two species do not allow for a straightforward comparison of their diffusion coefficients using Stokes' law based on the assumption of strictly spherical particles. Nevertheless, the overall size of DS^- is considerably larger than that of BTAH, and can represent itself as an even larger species when it forms micelles in the solution [31]. This is also evident in the relative thicknesses of BTAH and DS^-monolayer films (8–10 and 15–20 Å, respectively [7]) typically found on metal electrode substrates. Based on these considerations, the relatively larger values of $\sigma_a(DS^-)$ observed in Table 1 can be linked with slower diffusion of this species compared to that of BTAH. The mutually comparable values of σ_a found in solutions (d) and (e) suggest that in the BTAH-DS^- mixed electrolyte, diffusion limited mass transfer of adsorbates is rate limited by that of the larger species DS^- in the mixture [16].

For the Ref solution (a), R_p (220 Ω cm^2) found from EIS is consistently on the same order of the corresponding R_p (300 Ω cm^2) obtained from DC LPR measurements. The observed discrepancy between the two values is not unusual considering that the low frequency limit of FT-EIS used here is rather high compared to those generally used for AC measurement of polarization resistances [16]. In order to explain why R_p in the presence of the inhibitors is not detected in the FT-EIS data, it is necessary to compare the electrical admittances of the adsorption and polarization reactions (measured in the same DC voltage range). To do this, let us consider a situation where R_p is introduced as an additional branch parallel to the R_a–W_a branch in Fig. 7C. In this case, the admittance (denoted here as Y_{ap}) of the combined adsorption and polarization branches has the form: $Y_{ap} = Y'_{ap} + jY''_{ap} = \left[Y'_a + \left(1/R_p\right)\right] + jY''_a$. Here, Y'_{ap} and Y''_{ap} are the real and imaginary parts of Y_{ap}, respectively; Y'_a and Y''_a are the corresponding components of the admittance (Y_a) of the adsorption branch alone;$Y'_a = (Z'_a/|Z_a|^2)$ and $Y''_a = -(Z''_a/|Z_a|^2)$. The real and imaginary parts of the adsorption impedance Z_a are denoted as Z'_a and Z''_a, respectively. From Fig. 7C, $Z'_a = [R_a + (\sigma_a\omega^{-1/2})]$, and $-Z''_a = (\sigma_a\omega^{-1/2})$. By using the last two expressions in the above definition of Y'_a, the condition for not detecting R_p in EIS can be written as:

$$Y'_a = \frac{R_a + (\sigma_a\omega^{-1/2})}{[R_a + (\sigma_a\omega^{-1/2})]^2 + (\sigma_a\omega^{-1/2})^2} \gg \frac{1}{R_p}, \qquad (8)$$

where the polarization conductance ($1/R_p$) represents a measure of the overall rate of surface layer dissolution.

Since Y'_a decreases with decreasing values of ω, it is sufficient to check the above inequality only at the smallest value of Y'_a at the lowest angular frequency [2π (100 Hz)] of the impedance spectrum [15]: Using this frequency, and the values of σ_a and R_a from Table 1, we calculate Y'_a from Eq. 8; the results for the different experimental solutions are listed in the fifth row of Table 1. In the seventh row of Table 1, we also list the values of ($1/R_p$) calculated using the results of DC LPR measurements from Fig. 3. For all the inhibitor solutions (b–e), the value of ($1/R_p$) is at least an order of magnitude smaller than the corresponding Y'_a, and clearly satisfies Eq. 8. Thus in EIS, the R_a–W_a branch provides a low-resistance shunt for the AC current, avoiding the parallel high-resistance path of R_p. This explains why R_p in the presence of dissolution inhibitor adsorbates (that is, at finite values of Z_a) is too large to be detected in our FT-EIS measurements.

4 Conclusion

Using DC and AC electrochemical techniques, we have tested the surface dissolution inhibition efficiencies of ADS and BTAH on Cu in H_2O_2 containing acidic solutions of β-alanine. The results indicate that for ECMP applications, effective suppression of Cu dissolution can be achieved in this system by using 5 mM BTAH. Similar results can also be obtained by lowering further the BTAH concentration down to 1 mM, and mixing it with 3 mM ADS. The (potentially defect-causing) BTAH can be eliminated altogether from the experimental solution using 3 mM ADS alone as the inhibitor. While the latter system involves a moderate sacrifice of the dissolution inhibition efficiency, based on our recent findings [13] it might provide a better overall combination of scratch-free polishing and dissolution suppression. Based on the results of our DC LSV experiments, we have presented a reaction scheme for the chemical/electrochemical mechanisms of surface dissolution by β-alanine and H_2O_2 (and surface protection by BTAH and ADS). The EECs obtained from AC FT-EIS emerged in full agreement with these proposed surface reactions. The EECs obtained from EIS indicated essentially comparable adsorption resistances of BTAH and ADS on Cu/Cu_2O, although the diffusion characteristics (Warburg impedances) of the two inhibitor species in the solution were different due to their different molecular sizes. Furthermore, utilizing the high sensitivity of EIS to the relative rates of simultaneously occurring parallel surface reactions, we have demonstrated how the polarization resistance of Cu dissolution drastically increased in the presence of dissolution inhibitor adsorbates.

Acknowledgement We thank the School of Arts and Sciences of Clarkson University for financial support for this work, and Mr. Jianping Zheng for technical assistance.

References

1. Liu FQ, Du T, Duboust A, Tsai S, Hsu WY (2006) J Electrochem Soc C377:153
2. Huo J (2007) In: Li Y (ed) Microelectronic applications of chemical mechanical planarization. Wiley, New York, p 295
3. Goonetilleke PC, Roy D (2007) Mater Lett 61:380
4. Goonetilleke PC, Roy D (2005) Mater Chem Phys 94:388
5. Goonetilleke PC, Babu SV, Roy D (2005) Electrochem Solid-State Lett 8:G190
6. Hong Y, Roy D, Babu SV (2005) Electrochem Solid-State Lett 8:G297
7. Hong Y, Devarapalli VK, Roy D, Babu SV (2007) J Electrochem Soc 154:H 444
8. Hong Y, Patri UB, Ramakrishnan S, Roy D, Babu SV (2005) J Mater Res 20:3413
9. Ein-Eli Y, Starosvetsky D (2007) Electrochim Acta 52:1825
10. Robinson K (2006) In: Oliver MR (ed) Chemical mechanical planarization of semiconductor materials. Springer, New York, p 215
11. Edgar TF, Butler SW, Campbell WJ, Pfeiffer C, Bode C, Hwang SB, Balakrishnan KS, Hahn J (2000) Automatica 36:1567
12. Patri UB, Aksu S, Babu SV (2006) J Electrochem Soc 153:G650
13. Pandija S (2007) PhD Thesis, Clarkson University
14. Patri UB (2006) PhD Thesis, Clarkson University
15. Garland JE, Pettit CM, Roy D (2004) Electrochim Acta 49:2623
16. Barsoukov E, Macdonald JR (2005) In: Impedance spectroscopy: theory, experiment, and applications. Wiley, New York
17. Kelly RG, Scully JR, Shoesmith DW, Buchheit RG (2003) In: Electrochemical techniques in corrosion science and engineering. Marcel Dekker, New York
18. Tamilmani S, Huang W, Raghavan S, Small R (2002) J Electrochem Soc 149:G638
19. Hernandez J, Wrschka P, Oehrlein GS (2001) J Electrochem Soc 148:G389
20. Cohen SL, Brusic VA, Kaufman FB, Frankel GS, Motakef S, Rush B (1990) J Vac Sci Technol A 8:2417
21. Tromans D (1998) J Electrochem Soc 145:L24
22. Yeung H, Chan H, Weaver MJ (1999) Langmuir 15:3348
23. Sayed SY, El-Deab MS, El-Anadouli BE, Ateya BB (2003) J Phys Chem 107:5575
24. Assiongbon KA, Emery SB, Gorantla VRK, Babu SV, Roy D (2006) Corrosion Sci 48:372
25. Oh YJ, Park GS, Chung CH (2006) J Electrochem Soc 153:G617
26. Gorantla VRK, Assiongbon KA, Babu SV, Roy D (2005) J Electrochem Soc 152:G404
27. Lu J, Garland JE, Pettit CM, Babu SV, Roy D (2004) J Electrochem Soc 151:G717
28. Subramanian R, Lakshminarayanan V (2002) Corrosion Sci 44:535
29. Assiongbon KA, Emery SB, Pettit CM, Babu SV, Roy D (2004) Mater Chem Phys 86:347
30. Sluyters-Rebach M, Sluyters JH (1970) In: Bard A (ed) Electroanal chemistry, vol 4. Marcel Dekker, New York
31. Goonetilleke PC, Roy D (2008) Appl Surf Sci 254:2696